Necrotic core in EMT6/Ro tumour spheroids: Is it caused by an ATP deficit?

Alessandro Bertuzzi, Antonio Fasano, Alberto Gandolfi, Carmela Sinisgalli

www.elsevier.com/locate/yjtbi

Necrotic core in EMT6/Ro tumour spheroids: Is it caused by an ATP deficit?

Alessandro Bertuzzi, Antonio Fasano, Alberto Gandolfi, Carmela Sinisgalli

PII: S0022-5193(09)00454-8
DOI: doi:10.1016/j.jtbi.2009.09.024
Reference: YJTBI 5715

To appear in: *Journal of Theoretical Biology*

Received date: 17 February 2009
Revised date: 10 September 2009
Accepted date: 18 September 2009

Cite this article as: Alessandro Bertuzzi, Antonio Fasano, Alberto Gandolfi and Carmela Sinisgalli, Necrotic core in EMT6/Ro tumour spheroids: Is it caused by an ATP deficit?, *Journal of Theoretical Biology*, doi:10.1016/j.jtbi.2009.09.024

Necrotic core in EMT6/Ro tumour spheroids: is it caused by an ATP deficit?

Alessandro Bertuzzi[1], Antonio Fasano[2], Alberto Gandolfi[1], Carmela Sinisgalli[1]

[1]Istituto di Analisi dei Sistemi ed Informatica "A. Ruberti" - CNR
Viale Manzoni 30, 00185 Roma, Italy
e-mail: bertuzzi@iasi.cnr.it gandolfi@iasi.cnr.it sinisgalli@iasi.cnr.it

[2]Dipartimento di Matematica "U. Dini", Università di Firenze
Viale Morgagni 67/A, 50134 Firenze, Italy
e-mail: fasano@math.unifi.it

Abstract

Although commonly related to nutrient deprivation, the cause of the formation of the necrotic core in the multicellular tumour spheroids is still a controversial issue. We propose a simple model for the cell ATP production that assumes glucose and lactate as the only fuel substrates, and describes the main reactions occurring in the glycolytic and the oxidative pathways. Under the key assumption that cell death occurs when ATP production falls to a critical level, we formulate a multiscale model that integrates the energy metabolism at the cellular level with the diffusive transport of the metabolites in the spheroid mass. The model has been tested by predicting the measurements of the necrotic radius obtained by Freyer and Sutherland (1986a) in EMT6/Ro spheroids under different concentrations of glucose and oxygen in the culture medium. The results appear to be in agreement with the hypothesis that necrosis is caused by ATP deficit.

Keywords: tumour spheroid; necrosis; energy metabolism; ATP; diffusive transport; free boundary problems

1 Introduction

Poorly vascularized tumours show the occurrence of necrotic regions that have been mainly correlated to the deprivation of oxygen (Thomlinson and Gray, 1955, Tannock, 1968, Höckel and Vaupel, 2001). Investigations on *in vitro* growing tumour spheroids have been useful to characterize the dependence of necrosis formation on the external environment (Sutherland, 1988). During the growth of the spheroid the fraction of proliferating cells decreases, the cells in the inner region become deprived of oxygen, glucose and other nutrients whereas metabolic waste accumulates, and the formation of a necrotic core is observed. In an advanced stage of growth, indeed, spheroids show an outer viable rim (whose thickness ranges from about 100 to 250 μm) that surrounds the necrotic core. Because of the degradation of dead cells in the necrotic core (Folkman and Hochberg, 1973), the spheroid eventually attains a limiting size with a final diameter of 1-3 mm.

The spheroid growth has been described by a variety of mathematical models using either a continuum or a discrete approach (see Araujo and McElwain, 2004, for a comprehensive review). Almost all these models assumed that cell proliferation and cell death depend on the concentration of a single critical chemical that diffuses from the external medium into the cell aggregate. The diffusion of glucose, oxygen, lactate and other substrates has been included in a spheroid model proposed by Casciari et al. (1992). In that model, the cell proliferation rate was taken as an empirical function of glucose, oxygen and hydrogen ion concentrations. Both glucose and oxygen transport and consumption were included in discrete models (Schaller and Meyer-Hermann, 2005, Jiang et al., 2005) and in a continuum model of the spheroid growth (Schaller and Meyer-Hermann, 2006).

The hypothesis that the formation of necrotic regions is caused by a deficit in ATP production was adopted in a model of cell population growth in a tridimensional (sandwich) culture (Hlatky et al., 1988). More recently the cell energy metabolism, i.e. the intracellular ATP production, has been incorporated in continuous models of spheroid (Venkatasubramanian et al., 2006) and tumour cord growth (Astanin and Tosin, 2007), as well as in cellular automata tumour growth models (Smallbone et al., 2007, Gerlee and Anderson, 2008). Bertuzzi et al. (2007) proposed a simple mathematical model of cell ATP production that accounts for the main reactions occurring in the glycolytic and the oxidative pathways. The formation of the necrotic core in spheroids was described in that paper by assuming that cell death occurs when the ATP production rate falls below a critical threshold. This assumption led us to consider the diffusion free boundary problem for the concentrations of glucose, lactate and oxygen inside the spheroid viable rim.

In the present paper, our previous model of cell energy production is modified by simplifying the description of lactate transport and by adopting a more realistic assumption on pyruvate flux toward the Krebs cycle. Moreover, the diffusion of the nutrients in an unstirred layer surrounding the spheroid surface has been taken into account. The model of necrosis formation, based on the threshold on ATP production rate, has been applied to predict the measurements of the necrotic radius obtained by Freyer and Sutherland (1986a) by culturing EMT6/Ro spheroids under different concentrations of glucose and oxygen in the culture medium.

2 A simple mathematical model of ATP production

Although the *in vivo* cell energy metabolism involves glucose, fatty acids and amino acids, we only consider here glucose and lactate, so disregarding other energetic substrates possibly contained in the medium. The basic biochemical reactions of glucose metabolism are depicted in Fig. 1 (see e.g. Stryer, 1988) and are briefly described in the Appendix A, where the relationships (1) and (2) below are derived.

In particular, when the intracellular concentrations are constant in time, and under the hypothesis that glucose, lactate and oxygen are the only metabolites exchanged with the extracellular space, the stoichiometry of the metabolic reactions imposes the following relationship among the consumption rates (mol·cell^{-1}·s^{-1}) of these compounds:

$$f_O = 6f_G + 3f_L\,, \tag{1}$$

where $f_O > 0$ and $f_G > 0$ are the consumption rates of O_2 and glucose, respectively, and f_L is the consumption rate of lactate. Note that f_L can also be negative because, according to the reaction (A.2), there can be a net production of lactate. The production rate of ATP[1], f_{ATP}, can be expressed in terms of the above rates. Denoting by η_1 and η_2 the efficiency of the phosphorylation of ADP into ATP related to the oxidation of NADH and, respectively, $FADH_2$, the relation

$$f_{ATP} = 2f_G + (5\eta_1 + \eta_2 + 1)f_O/3 \tag{2}$$

follows (see the Appendix A).

Equations (1)-(2) give the relations among the metabolic fluxes that are implied by the stoichiometry of reactions, but say nothing on the extent of these fluxes. To our aims, moreover, it is necessary to express the consumption/production rates in terms of the extracellular concentrations. Let us consider a cell surrounded by a medium in which glucose, oxygen and lactate have constant concentrations σ_G, σ_O and, respectively, σ_L. The respective intracellular concentrations will be denoted as $\bar{\sigma}_G$, $\bar{\sigma}_O$, and $\bar{\sigma}_L$. We assume: *(i)* glucose uptake follows a Michaelis-Menten kinetics and all glucose taken up by cells is consumed (Casciari et al., 1992, Venkatasubramanian et al., 2006); *(ii)* the exchange of pyruvate with the extracellular medium is disregarded; *(iii)* transmembrane transport of lactate is non-saturable in the concentration range of interest, and is driven by the gradient of lactate concentration; *(iv)* because of the high permeability of cell membrane to oxygen (Alberts et al., 1994), oxygen concentration inside the cell is equal to the extracellular concentration; *(v)* the pyruvate flow toward the Krebs cycle is a saturable function of pyruvate and oxygen concentrations (see also Aubert and Costalat, 2005).

Experimental data (Freyer and Sutherland, 1985, Casciari et al., 1992, Schroeder et al., 2005) have shown that glucose consumption increases when oxygen concentration decreases (the so-called Pasteur effect) and that, at physiological pH, oxygen consumption increases when glucose concentration decreases (the so-called Crabtree effect). Expressions for the glucose and oxygen consumption including the above effects were proposed on an empirical basis (Casciari et al., 1992). These effects seem to depend on the pH of cell environment: for

[1]Abbreviations: ATP, adenosine triphosphate; ADP, adenosine diphosphate; P_i, inorganic orthophosphate; GTP, guanosine triphosphate; GDP, guanosine diphosphate; NAD^+, nicotinamide adenine dinucleotide (oxidized form); NADH, nicotinamide adenine dinucleotide (reduced form); FAD, flavin adenine dinucleotide (oxidized form); $FADH_2$, flavin adenine dinucleotide (reduced form); Ac-CoA, acetyl-CoA.

instance, the Crabtree effect disappears in an acidic environment. Although the production of H^+ ions is related to lactic acid production, the description of pH changes is complicated by the presence of an intracellular buffer (see the mathematical models in Casciari et al., 1992, and Webb et al., 1999). Since a mechanistic representation of these phenomena appears to be rather complex, they are neglected in our model.

For lactate transport, it is known that most of its influx and efflux occur through monocarboxylate transporters (MCTs) which exhibit saturable kinetics (Poole and Halestrap, 1993). In Ehrlich tumour cells the Michaelis-Menten constant, K_m, of transport kinetics has been found to be 20 mM at 37 °C and pH 7.2 (Spencer and Lehninger, 1976) and, with a different technique, 5.34 mM in the same conditions (Carpenter and Halestrap, 1994). In the mammary carcinoma MDA-MB231, high affinity (MCT2) and low affinity (MCT4) transporters have been evidenced (Wang and Morris, 2007), with a prevalent flux through MCT4 ($K_m = 21.3$ mM). The K_m values have been found to be highly pH dependent, with K_m decreasing with acidity (Dimmer et al., 2000). So, in the presence of a difference between extracellular and intracellular pH, an asymmetric flux could occur. In the present paper we neglect this possible asymmetry, at variance with our previous paper (Bertuzzi et al., 2007), and the high K_m values reported above lead us to assume a simple non-saturable kinetics for lactate transport.

On the basis of the above assumptions, the rate of glucose consumption is given by

$$f_G(\sigma_G) = F_G \frac{\sigma_G}{K_G + \sigma_G}, \tag{3}$$

where F_G is the maximal rate of uptake and K_G is the Michaelis-Menten constant. For the intracellular concentrations of pyruvate and lactate we write the following equations:

$$v\frac{d\bar{\sigma}_P}{dt} = 2f_G(\sigma_G) - \psi(\bar{\sigma}_P, \bar{\sigma}_L) - \phi_P(\bar{\sigma}_P, \sigma_O), \tag{4}$$

$$v\frac{d\bar{\sigma}_L}{dt} = \psi(\bar{\sigma}_P, \bar{\sigma}_L) + v\,h(\sigma_L - \bar{\sigma}_L), \tag{5}$$

where v is the cell volume, ψ is the net flow of pyruvate to lactate, ϕ_P is the pyruvate flow toward the Krebs cycle, and h is the transfer coefficient of lactate transmembrane transport. Although the reversible reaction between pyruvate and lactate is an enzymatic reaction, we simply represent it by a first-order reaction, writing

$$\psi(\bar{\sigma}_P, \bar{\sigma}_L) = v(k_+\bar{\sigma}_P - k_-\bar{\sigma}_L), \tag{6}$$

where k_+ and k_- are the forward and, respectively, the backward rate constants. The complex chain of reactions in the Krebs cycle and the electron transport system that lead to pyruvate oxidation, is summarized in the simplest way according to assumption *(v)*:

$$\phi_P(\bar{\sigma}_P, \sigma_O) = F_P \frac{\bar{\sigma}_P}{K_P + \bar{\sigma}_P} \frac{\sigma_O}{K_O + \sigma_O}. \tag{7}$$

Expression (7) modifies the previous expression for ϕ_P adopted in Bertuzzi et al. (2007), where the pyruvate flow toward the Krebs cycle was taken proportional to the product of pyruvate and oxygen concentrations. The expression (7) accounts for the saturative behaviour of enzymatic reactions in the pyruvate oxidation pathway.

Using Eqs. (3)-(7), the intracellular concentration of pyruvate at the steady state can be derived in terms of the extracellular concentrations. From (5)-(6) we derive:

$$\bar{\sigma}_L = \frac{k_+}{k_- + h}\,\bar{\sigma}_P + \frac{h}{k_- + h}\sigma_L\,. \tag{8}$$

To write the following equations in a more compact form, we define the functions

$$M(\sigma_O) = \frac{\sigma_O}{K_O + \sigma_O}\,,$$

$$N(\sigma_G, \sigma_L) = 2f_G(\sigma_G) + p_1\sigma_L\,,$$

and the parameter combinations

$$p_1 = \frac{k_- h}{k_- + h}v\,, \qquad p_2 = \frac{k_+ h}{k_- + h}vK_P\,.$$

From (4), taking into account (5), (7) and (8), we then obtain

$$\begin{aligned}\bar{\sigma}_P = \; & -\; \frac{K_P}{2p_2}[p_2 + F_P M(\sigma_O) - N(\sigma_G, \sigma_L)] \\ & +\; \frac{K_P}{2p_2}\Big(\big[p_2 + F_P M(\sigma_O) - N(\sigma_G, \sigma_L)\big]^2 + 4p_2 N(\sigma_G, \sigma_L)\Big)^{1/2}\,.\end{aligned} \tag{9}$$

As seen in Appendix A, the stoichiometry of the reactions at the steady state gives for the oxygen consumption rate, f_O, the equation

$$f_O = 3\phi_P\,.$$

Therefore, dropping the arguments of the functions $M(\sigma_O)$ and $N(\sigma_G, \sigma_L)$, we can write:

$$f_O(\sigma_G, \sigma_L, \sigma_O) = \frac{3}{2}\Big(p_2 + F_P M + N - \big([p_2 + F_P M + N]^2 - 4F_P MN\big)^{1/2}\Big). \tag{10}$$

Note that f_O is zero for $\sigma_O = 0$ and

$$\left.\frac{df_O}{d\sigma_O}\right|_{\sigma_O=0} = 3\,\frac{N}{p_2 + N}\,\frac{F_P}{K_O}\,.$$

For σ_O increasing, f_O attains the saturation value:

$$f_{O_{max}}(\sigma_G, \sigma_L) = \frac{3}{2}\Big(p_2 + F_P + N - \big([p_2 + F_P + N]^2 - 4F_P N\big)^{1/2}\Big)\,. \tag{11}$$

The oxygen consumption rate increases with N, and then with the glucose consumption and lactate uptake, but it is always less than $3F_P$ as expected from (7). When $4F_P N \ll (p_2 + F_P + N)^2$ and $p_2 + N > F_P$ we have $4F_P MN \ll (p_2 + F_P M + N)^2$ for any $\sigma_O > 0$, and Eq. (10) can be approximated by the expression

$$f_O(\sigma_G, \sigma_L, \sigma_O) \simeq 3\frac{F_P MN}{p_2 + F_P M + N}\,,$$

that gives an easier insight of (10) and (11). Moreover, if $p_2 \gg F_P + N$, the previous equation can be further approximated as

$$f_O(\sigma_G, \sigma_L, \sigma_O) \simeq \gamma NM = \gamma\big(2f_G(\sigma_G) + p_1\sigma_L\big)\frac{\sigma_O}{K_O + \sigma_O}\,, \tag{12}$$

where $\gamma = 3F_P/p_2$.

The equation for the rate of lactate consumption, $f_L(\sigma_G, \sigma_L, \sigma_O)$, follows from (1) written as

$$f_L = \frac{1}{3}f_O - 2f_G\,, \tag{13}$$

with f_G and f_O defined above. f_L may be positive or negative according to the oxygen concentration: when $\sigma_O \to 0$ we will have $f_L < 0$, that is, lactate production.

In view of the expressions of $M(\sigma_O)$ and $N(\sigma_G, \sigma_L)$, when the equation (10) for f_O is adopted, the consumption rates f_G, f_L and f_O depend on the following parameters and parameter combinations: F_G, K_G, F_P, K_O, p_1 and p_2. When the approximation (12) is used, the model parameters reduce to F_G, K_G, γ, K_O and p_1.

Figure 2 gives an example of the profile of the oxygen consumption rate as a function of oxygen concentration, according to (10), for an assigned concentration of extracellular lactate and three concentrations of glucose. The behaviour of the maximal value of f_O as a function of the extracellular glucose and lactate concentrations is depicted by Figure 3. The profile of lactate production/consumption rate as a function of oxygen concentration is shown in Fig. 4 for two values of extracellular glucose and three values of lactate concentration. In the absence of extracellular glucose (left panel), lactate is consumed with a rate that increases with its concentration. When glucose is present, lactate can be either produced or consumed depending on the extracellular lactate concentration. The right panel exemplifies this behaviour for $\sigma_G = 5\,\mu$M. However, when oxygen concentration is small enough, lactate is produced in the presence of glucose irrespective of the value of σ_L. At $\sigma_O = 0$, in fact, it is $f_L = -2f_G$.

Experimental evidences have suggested that energy metabolism of tumour cells mainly relies on the glycolytic pathway for the ATP production, thus exhibiting enhanced lactate production and the formation of an acidic environment. These observations led O. Warburg to the notion of the glycolytic phenotype of cancer cells (Warburg, 1956). Recently, however, this view has been questioned by stressing that cells may rely on glycolysis because of the prevailing hypoxic conditions in tumours (Guppy et al., 2002). In our model, the balance between the glycolytic and the aerobic ATP production is governed by the parameters k_+, F_P and K_P. From Eqs. (2) and (10), we see that if the product k_+K_P is large and F_P is small, the aerobic production of ATP is small even in the presence of high oxygen concentrations, and thus the cells would express a glycolytic phenotype. The fraction of the total ATP produced by glycolysis at high oxygen concentration ($M(\sigma_O) = 1$) is plotted in Fig. 5 as a function of F_P for three values of parameter p_2. Values of this fraction close to the unity indicate a glycolytic phenotype. The curves show the increase of this fraction, and then the transition to the glycolytic phenotype, as F_P decreases and the product k_+K_P increases.

3 Development of central necrosis in multicellular spheroids

We consider a spheroid of radius R, in which the nutrient consumption rates of all viable cells depend on the concentrations of the chemicals according to the expressions given in the previous section. Since the growth dynamics of the spheroid is much slower than the process of diffusion of the nutrients, we will consider the diffusion process in spherical symmetry to be at the quasi-steady state at any time. Of course all the derivatives σ_i', $i = G, L, O$, of the extracellular concentrations $\sigma_G(r)$, $\sigma_L(r)$, $\sigma_O(r)$ vanish for $r = 0$ by symmetry (whether or not a necrotic core is present).

We assume that all cells die when f_{ATP}, as given by (2), falls to a threshold value f_N, and we suppose that the impairment of the ATP production is the only cause of formation of the necrotic core. According to this hypothesis, the viable region of the spheroid is defined by the inequality

$$f_{ATP}(r) > f_N \,.$$

We obviously assume that the concentrations at the boundary R are such that $f_{ATP}(R) > f_N$. In the absence of a necrotic core, the viable region will extend from $r = 0$ to $r = R$. In the viable region the concentrations σ_G, σ_L, σ_O obey the equations

$$D_i \frac{1}{r^2}\frac{\partial}{\partial r}\left(r^2 \frac{\partial \sigma_i}{\partial r}\right) = n f_i \,, \quad i = G, L, O \,, \tag{14}$$

where D_i denote the effective diffusivities and $n = \nu^*/v$, with ν^* the cell volume fraction assumed to be constant, is the number of cells per unit volume. The quantities f_i, $i = G, L, O$, in (14) are the consumption/production rates per cell defined in the previous section by Eqs. (3), (13) and (10) (or (12)), respectively. For simplicity, the possible changes in the consumption rates between proliferating and quiescent cells are disregarded. We remark that the values of the diffusivities (see Table 1) guarantee that the contribution of the extracellular liquid flow to metabolite transport is negligible.

Experimental observations that evidenced the presence of concentration gradients in a layer surrounding the surface of tumour spheroids (Mueller-Klieser and Sutherland, 1982, Mueller-Klieser, 1984, Groebe and Mueller-Klieser, 1991), led us to prescribe the concentrations in the culture medium at a fixed distance L from the spheroid surface. These concentrations obey the following equations:

$$D_i^w \frac{1}{r^2}\frac{\partial}{\partial r}\left(r^2 \frac{\partial \sigma_i}{\partial r}\right) = 0 \,, \quad i = G, L, O \,, \quad R < r < R + L \,, \tag{15}$$

$$\sigma_i(R + L) = \sigma_i^* > 0 \,, \quad i = G, O \,, \qquad \sigma_L(R + L) = \sigma_L^* \geq 0 \,, \tag{16}$$

$$\sigma_i(R^-) = \sigma_i(R^+) \,, \quad D_i \sigma_i'(R^-) = D_i^w \sigma_i'(R^+) \,, \quad i = G, L, O \,, \tag{17}$$

where D_i^w denote the diffusivities in the medium, and continuity of concentrations and fluxes is imposed at $r = R$.

In the presence of a necrotic core, we denote by ρ_N the radius of the necrotic region. In this case the viable region reduces to a rim $\rho_N < r < R$. At the necrotic boundary $r = \rho_N$, we will have the conditions

$$f_{ATP}(\rho_N) = f_N \,, \tag{18}$$

$$\sigma_i'(\rho_N) = 0 \,, \qquad i = G, L, O \,. \tag{19}$$

In the necrotic core the nutrient concentrations are constant and $f_{ATP} = 0$.

In Bertuzzi et al. (2007), the concentrations σ_i^* in the culture medium were simply prescribed at the boundary R:

$$\sigma_i(R) = \sigma_i^* > 0\,, \quad i = G, O\,, \qquad \sigma_L(R) = \sigma_L^* \geq 0\,. \tag{20}$$

In that case we proved the following results:

- For R sufficiently large, the inequality $f_{ATP}(r) > f_N$ cannot hold in the whole interval $(0, R)$.
- For R sufficiently large, there exists one and only one solution $\sigma_G(r)$, $\sigma_L(r)$, $\sigma_O(r)$, ρ_N of the free boundary problem defined by Eqs. (14), (18), (19) and (20).

Therefore, given the concentrations σ_i^* and the threshold f_N, an increasing function $\rho_N = \Phi(R)$ is defined for $R > R_N > 0$, with $\rho_N = 0$ for $R = R_N$, where R_N is the spheroid radius at which the central necrosis starts to appear.

We note that the existence proofs in Bertuzzi et al. (2007) remain valid even if the consumption rates are not precisely the ones there proposed, but just possess the same qualitative properties as those proposed here. Moreover, it can be easily seen that the above existence results still hold for the free boundary problem considered in the present paper, which is defined by Eqs. (14), (18), (19) and (15–17).

4 Necrotic core in EMT6/Ro spheroids

The growth characteristics and the metabolism of the EMT6/Ro spheroid (mouse mammary carcinoma cells) have been extensively investigated (Mueller-Klieser and Sutherland, 1982, Mueller-Klieser, 1984, Freyer and Sutherland, 1985, Freyer and Sutherland, 1986a, Casciari et al., 1988, Freyer, 1988, Walenta et al., 1990, Freyer et al., 1991, Casciari et al., 1992, Casciari et al., 1992a). In Freyer and Sutherland (1986a) in particular, the radius of the necrotic core for spheroids of different size and under different oxygen and glucose concentrations in the medium were reported. These data have been used to evaluate the predictive capability of our model.

The values of a subset of model parameters were assigned according to the literature data (see Table 1). Freyer and Sutherland (1985) reported, for an exponentially growing monolayer culture of EMT6/Ro cells with 5.5 mM glucose, the following values of the glucose consumption rate: 18×10^{-17} mol/(cell·s) when oxygen concentration was 0.28 mM and 25×10^{-17} mol/(cell·s) when oxygen concentration was 0.07 mM. This finding suggested to take for F_G the mean of the above values. In the same paper, the oxygen consumption rate per cell is also reported. In particular, for an oxygen concentration of 0.28 mM and glucose concentration of 5.5 mM, the value of 8.3×10^{-17} mol/(cell·s) has been found. We used this data as a constraint on the value of the unknown parameters. The thickness of the unstirred layer around the spheroid has been found to range from $60 - 80\,\mu$m (Groebe and Mueller-Klieser, 1991) to $100 - 200\,\mu$m (Mueller-Klieser, 1984), hence we assumed $L = 80\,\mu$m.

The other parameters and parameter combinations of the biochemical model and the ATP threshold, f_N, were instead determined by minimizing the deviation from the experimental data. Let θ be the vector of the parameters to be estimated. We denote

by j, $j = 1, \ldots, 8$, the different conditions in which the spheroids were grown in Freyer and Sutherland (1986a): $j = 1, \ldots, 4$ refer to experiments with $\sigma_O^* = 0.07\,\mathrm{mM}$ and σ_G^* equal to 0.8, 1.7, 5.5 and 16.5 mM, respectively; $j = 5, \ldots, 8$ indicate experiments with $\sigma_O^* = 0.28\,\mathrm{mM}$ and σ_G^* as above. For all the experiments we assumed $\sigma_L^* = 0$. Let us define by X_i^j, Y_i^j, $i = 1, \ldots, N_j$, the i-th measured values of the necrotic core radius, ρ_N, and respectively of the spheroid radius, R, in the j-th experiment. By $\Phi_j^{-1}(\rho_N)$ we denote the function that gives the spheroid radius, R, for which the radius of the necrotic core is ρ_N under the experimental condition j. This function is well defined since the function Φ is increasing. The optimal fitting was achieved by minimizing the index

$$J(\theta) = \sum_{j=1}^{8} \sum_{i=1}^{N_j} (\Phi_j^{-1}(X_i^j; \theta) - Y_i^j)^2 \,. \tag{21}$$

The choice of the index (21) deserves some comments. A more intuitive choice would be that of fitting the measurements of the necrotic radius by the function $\tilde{\Phi}$ defined as

$$\tilde{\Phi}(\theta) = \begin{cases} 0\,, & R \le R_N(\theta) \\ \Phi(R;\theta)\,, & R > R_N(\theta)\,. \end{cases}$$

In this way, however, the quadratic deviations for the measurements with R values smaller than $R_N(\theta)$ have zero derivative with respect to θ, and then do not contribute to the selection of the descent direction in the minimization. This problem has been avoided by using the index (21). For the minimization, we used a global-search derivative-free algorithm, reported in Liuzzi et al. (2003), that searches the minimum in a rectangular box of the parameter space whose boundaries must be a priori assigned. The function Φ_j^{-1} for a given ρ_N was computed according to the steps briefly described in Appendix B.

Firstly, adopting Eq. (10) for the oxygen consumption rate, the estimation of the parameters F_P, p_1, p_2, and of the threshold f_N, was attempted. The minimization was performed under the constraint that the prediction, $q_O(\theta)$, of the oxygen consumption rate for $\sigma_G = 5.5\,\mathrm{mM}$, $\sigma_L = 0$, $\sigma_O = 0.28\,\mathrm{mM}$ met the measured value $Z_O = 8.3 \times 10^{-17}\,\mathrm{mol/(cell{\cdot}s)}$ (Freyer and Sutherland, 1985) within a prescribed tolerance. However, the parameters F_P, p_1, p_2 could not be reliably estimated, as different parameter sets were found to give similar fittings. In particular, the estimated values of p_2 were large enough to make approximation (12) feasible, so we used that approximation to fit the data. With the approximation (12) the estimation problem is considerably simplified since the quantity q_O only depends on the unknown parameter γ. By setting $q_O = Z_O$, we obtained for γ the value 0.198 (see Table 2). Therefore, the only parameters to be estimated were p_1 and f_N, and the fitting so obtained was found to be substantially equal to that obtained when using Eq. (10). The covariance matrix of the estimates was computed by the linearization method that yields

$$Cov(\hat{\theta}) = s^2 \left(\left. \frac{dg}{d\theta} \right|_{\hat{\theta}}^T \left. \frac{dg}{d\theta} \right|_{\hat{\theta}} \right)^{-1} ,$$

where $\hat{\theta}$ is the vector of the estimated parameters, $g(\theta)$ is the vector with components $\Phi_j^{-1}(X_i^j; \theta)$ for all i and j, and s^2 is the estimate of the (common) variance of the measurements, given by

$$s^2 = \frac{J(\hat{\theta})}{\sum_{j=1}^{8} N_j - m} \,,$$

with $m = 2$ being the number of unknown parameters.

The optimal prediction of the radius of the necrotic core as a function of the spheroid radius is shown in Fig. 6, together with the experimental data. It can be noted that the model reasonably predicts the clear dependence of the necrotic radius on the oxygen value in the medium at glucose 5.5 mM, and the small sensitivity to oxygen when glucose attains the extreme values of 0.8 and 16.5 mM. Less satisfactory is the fitting of the data at glucose 1.7 mM, particularly for the oxygen concentration of 0.07 mM when the data at glucose 0.8 and 1.7 mM are practically indistinguishable while the model exhibits a monotone dependence on σ_G^*. The optimal parameter values are reported in Table 2. As a comment to these values we note the following. The experimental data of lactate transport in Ehrlich tumour cells (Carpenter and Halestrap, 1994) indicate, for the ratio between maximal transport rate and Michaelis constant, the value $0.13\,\mathrm{s}^{-1}$. Assuming that the coefficient h in Eq. (5) is equal to this ratio, we obtain an upper limit of p_1, given by hv, equal to 37.0×10^{-14} liter/(cell·s), having taken $v = 2.86\times10^{-12}$ liter/cell (v was computed as ν^*/n taking n as in Table 1 and $\nu^* = 0.6$). Thus, the obtained value of p_1 satisfies the above upper bound. The ATP production rate at the surface of spheroids cultured with 5.5 mM glucose and 0.28 mM oxygen was computed, giving a range from 85 to 95×10^{-17} mol/(cell·s) at different R values. Thus the estimated value of the threshold f_N is close to half of this value.

Figure 7 reports the predicted profiles of metabolite concentrations and of the ATP production rate across a spheroid of radius 400 μm cultured with 5.5 mM glucose and 0.28 mM oxygen. The metabolite concentrations in the unstirred layer are also shown. A marked increase in ATP production rate in the middle of the viable rim can be noted. This maximum is due to the increase in the oxygen consumption rate caused by the increase in lactate concentration, see the definition of $N(\sigma_G, \sigma_L)$. The presence of a maximum of f_{ATP} internal to the viable rim matches the existence of an internal maximum of ATP concentration in EMT6/Ro spheroids as measured by bioluminescence (Walenta et al., 1990). The mean ATP production rate per cell over the viable rim was also computed as

$$\langle f_{ATP} \rangle = \frac{3}{R^3 - \rho_N(R)^3} \int_{\rho_N(R)}^{R} r^2 f_{ATP}(r)\, dr\,.$$

For R increasing from 250 to 1000 μm, the mean production rate was found to slightly decrease with R, ranging from 120 to 114×10^{-17} mol/(cell·s).

5 Concluding remarks

The model we propose appears to give a reasonable prediction of the radius of the necrotic core as measured in EMT6/Ro spheroids cultured in different conditions of oxygen and glucose (Freyer and Sutherland, 1986a). The main feature of the model is the assumption that the onset of necrosis is caused by an insufficient ATP production rate and this hypothesis, which is controversially discussed in the literature (Walenta et al., 2000), appears thus in agreement with the data considered. Attempts to predict these data by using a threshold on a single nutrient, oxygen or glucose, gave far worse results (not shown). Nuclear magnetic resonance measurements in EMT6/Ro spheroids showed that high energy phosphates remained at a normal steady level irrespective of the stage of spheroid growth

(Freyer et al., 1991). Under the assumption that the ATP content per cell is proportional to the ATP production rate, our model meets this observation as it predicts that the mean ATP production rate per cell is only slightly decreasing with the spheroid radius.

A limitation of the model is that the presence in the spheroids of quiescent cells (Freyer and Sutherland, 1986b), possibly with different rates of nutrient consumption, is disregarded. In principle, the model could be extended to take into account a quiescent cell population. However, since the transition to quiescence should be related to the availability of nutrients or, more strictly, to the energy production, this extension would require additional assumptions and parameters thus making the model validation more uncertain.

As mentioned above, experimental investigations on the EMT6/Ro cell line have shown the presence of the Pasteur and Crabtree effects, that is, the dependence of glucose and, respectively, oxygen consumption rates on the concentration of the other metabolite. The complex mechanisms that underlie these phenomena and their dependence on pH, however, have prevented us from including these effects in a relatively simple model.

Modelling the pH profile in the spheroid would thus be a valuable improvement, even in view of the possible role of acidity in inducing cell death, that suggests different hypotheses on the formation of the necrotic core. The relevance of pH has been pointed out, in fact, not only in connection with the invasive capacity of the tumour (Gatenby and Gawlinski, 1996, Smallbone et al., 2005, Fasano et al., 2009), but also in connection with the formation of the tumour necrotic regions (Smallbone et al., 2005, Bianchini and Fasano, 2009).

Appendix A. Glucose energy metabolism: main biochemical reactions and metabolic fluxes

As shown by Fig. 1 glycolysis is the first step of glucose metabolism, in which a sequence of enzymatic reactions converts 1 molecule of glucose into 2 molecules of pyruvate with the simultaneous net production of 2 ATP molecules and the conversion of 2 NAD^+ into 2 NADH molecules:

$$\mathrm{Glucose} + 2\mathrm{NAD}^+ + 2\mathrm{P_i} + 2\mathrm{ADP} \rightarrow 2\mathrm{Pyruvate} + 2(\mathrm{NADH} + \mathrm{H}^+) + 2\mathrm{ATP} + 2\mathrm{H_2O}\,. \quad \text{(A.1)}$$

Pyruvate may either be reversibly converted into lactate or undergo complete oxidation in the Krebs cycle and the associated electron transport system (ETS). The former reaction is given by

$$\mathrm{Pyruvate} + \mathrm{NADH} + \mathrm{H}^+ \rightleftharpoons \mathrm{Lactate} + \mathrm{NAD}^+\,. \quad \text{(A.2)}$$

Pyruvate oxidation occurs through multiple steps, but the net reaction may be written as follows:

$$\begin{aligned}\mathrm{Pyruvate} + 4\mathrm{NAD}^+ + \mathrm{FAD} + 3\mathrm{H_2O} + \mathrm{P_i} + \mathrm{GDP} \\ \rightarrow 3\mathrm{CO_2} + 4(\mathrm{NADH} + \mathrm{H}^+) + \mathrm{FADH_2} + \mathrm{GTP}\,.\end{aligned} \quad \text{(A.3)}$$

The NADH produced in the glycolytic step, the pyruvate→acetyl-CoA step and the Krebs cycle, together with the $FADH_2$ produced in the Krebs cycle, are oxidized in the so-called electron transport system:

$$10(\mathrm{NADH} + \mathrm{H}^+) + 2\mathrm{FADH_2} + 6\mathrm{O_2} \rightarrow 10\mathrm{NAD}^+ + 2\mathrm{FAD} + 12\mathrm{H_2O}\,. \quad \text{(A.4)}$$

In the above reaction, that refers to the oxidation of 1 glucose molecule, 2 NADH molecules derive from the pyruvate→acetyl-CoA step, 6 NADH from the Krebs cycle, and the remaining 2 molecules from the glycolytic step. We note that this reaction, together with (A.2), provides all the NAD^+ and FAD molecules required in reactions (A.1) and (A.3). The reactions in the ETS yield the energy necessary for the phosphorylation of ADP into ATP. The efficiency of this process appears to vary depending on cell type and cell condition. The transformation of 1 NADH molecule in NAD^+ provides energy for the formation, in average, of about 2.5 ATP molecules, whereas 1 $FADH_2$ generates about 1.5 ATP molecules (Hinkle et al., 1991). In addition, we remark that the GTP molecule produced in the Krebs cycle is equivalent to an ATP molecule.

Let us consider a cell at the steady state and assume that glucose, lactate and oxygen are the only metabolites exchanged with the extracellular space. Let ϕ_G, ϕ_P, ϕ_L^+, and ϕ_L^- denote the fluxes (mol·cell^{-1}·s^{-1}) of glucose to pyruvate, pyruvate to acetyl-CoA, pyruvate to lactate and, respectively, lactate to pyruvate.

Recalling (A.1)-(A.2), the net production rate of NADH in the reactions

$$\text{Glucose} \rightarrow \text{Pyruvate} \rightleftharpoons \text{Lactate}$$

is given by $2\phi_G - \phi_L^+ + \phi_L^-$, because when pyruvate is converted into lactate, 1 NADH molecule is consumed. Since the cumulative production rate of NADH and $FADH_2$ from pyruvate oxidation is $5\phi_P$, and each NADH or $FADH_2$ molecule requires $(1/2)O_2$ to be oxidized (see reaction (A.4)), for the oxygen consumption rate, f_O, we have:

$$f_O = \frac{5}{2}\phi_P + \phi_G - \frac{1}{2}\phi_L^+ + \frac{1}{2}\phi_L^- .$$

As the flux balance at the steady state give

$$\phi_P = 2\phi_G - \phi_L^+ + \phi_L^- , \tag{A.5}$$

it follows that

$$f_O = 3\phi_P . \tag{A.6}$$

Moreover, taking into account that

$$f_G = \phi_G , \qquad f_L = \phi_L^- - \phi_L^+ ,$$

from (A.5) and (A.6) we obtain equation (1):

$$f_O = 6f_G + 3f_L .$$

Denoting by η_1 and η_2 the mean number of ATP molecules generated as a consequence of the oxidation of 1 NADH and 1 $FADH_2$ molecules, respectively, from reactions (A.1)–(A.3) we can write the rate of ATP production, f_{ATP}, as

$$f_{ATP} = 2\phi_G + \phi_P + \eta_1(4\phi_P + 2\phi_G - \phi_L^+ + \phi_L^-) + \eta_2\phi_P .$$

Note that the second term in the right-hand side represents the production of GTP, considered equivalent to ATP. Since $\phi_P = f_O/3$, the above equation can be rewritten giving equation (2):

$$f_{ATP} = 2f_G + (5\eta_1 + \eta_2 + 1)f_O/3 .$$

Appendix B. Computation of the function Φ_j^{-1}

The computation of the function Φ_j^{-1} for a given ρ_N was performed according to the steps briefly described in the following. Preliminarily, each equation in (14) is rewritten as a system of two first-order differential equations for σ_i and σ_i'.

1. For any experimental value of ρ_N, fix an initial guess for $R = \Phi_j^{-1}(\rho_N)$ equal to $(\rho_N + R_{max})/2$, with R_{max} a suitable large value.

2. Find the values $\bar{\sigma}_i$, $i = G, L, O$, such that the Cauchy problem defined by Eqs. (14), (15), (17), with the initial conditions $\sigma_i(\rho_N) = \bar{\sigma}_i$ and (19), has a solution such that $\sigma_i(R + L) = \sigma_i^*$. This "shooting" step is performed in the following way.

   2a. Given a triple $\bar{\sigma}_i$, $i = G, L, O$, integrate Eqs. (14) with conditions $\sigma_i(\rho_N) = \bar{\sigma}_i$ and (19) on $[\rho_N, R]$, and continue the solutions up to the radius $R+L$ according to (15) and (17).

   2b. Minimize with respect to $\bar{\sigma}_i$ the index

$$I(\bar{\sigma}_G, \bar{\sigma}_L, \bar{\sigma}_O) = \sum_{i=G,L,O} (\sigma_i(R + L) - \sigma_i^*)^2 .$$

   The minimization is accomplished by the Levemberg-Marquardt algorithm.

3. Compute the ATP production rate at ρ_N, $f_{ATP}(\rho_N; R)$, using the $\bar{\sigma}_i$ values obtained at step 2b.

4. Find the solution with respect to R of the equation $f_{ATP}(\rho_N; R) = f_N$ by means of the bisection method, iterating steps 2 and 3 a suitable number of times (n=30).

Acknowledgements

The authors wish to thank Dr. G. Liuzzi for the precious help given in solving the optimization problem. The authors also acknowledge the work done by Drs. P. Nanci and P. Pasanisi in the software development. Finally, we thank the anonymous Referees for their constructive comments that allowed us to improve the paper.

References

Alberts, B., Bray, D., Lewis, J., Raff, M., Roberts, K., Wastson, J.D., 1994. Molecular Biology of the Cell, Garland Publishing, New York, Chap. 11.

Araujo, R.P., McElwain, D.L.S., 2004. A history of the study of solid tumour growth: the contribution of mathematical modelling. Bull. Math. Biol. 66, 1039–1091.

Astanin, S., Tosin, A., 2007. Mathematical model of tumour cord growth along the source of nutrient. Math. Model. Nat. Phenom. 2, 153–177.

Aubert, A., Costalat, R., 2005. Interaction between astrocytes and neurons studied using a matematical model of compartmentalized energy metabolism. J. Cereb. Blood Flow Metab. 25, 1476–1490.

Bertuzzi, A., Fasano, A., Gandolfi, A., Sinisgalli, C., 2007. ATP production and necrosis formation in a tumour spheroid model. Math. Model. Nat. Phenom. 2, 30–46.

Bianchini, L., Fasano, A., 2009. A model combining acid-mediated tumour invasion and nutrient dynamics. Nonlin. Anal. Real World Appl. 10, 1955–1975.

Carpenter, L., Halestrap, A.P., 1994. The kinetics, substrate and inhibitor specificity of the lactate transporter of Ehrlich-Lettre tumour cells studied with the intracellular pH indicator BCECF. Biochem. J. 304, 751–760.

Casciari, J.J., Sotirchos, S.V., Sutherland, R.M., 1988. Glucose diffusivity in multicellular tumor spheroids. Cancer Res. 48, 3905–3909.

Casciari, J.J., Sotirchos, S.V., Sutherland, R.M., 1992. Mathematical modelling of microenvironment and growth in EMT6/Ro multicellular tumour spheroids. Cell Prolif. 25, 1–22.

Casciari, J.J., Sotirchos, S.V., Sutherland, R.M., 1992a. Variations in tumor cell growth rates and metabolism with oxygen concentration, glucose concentration, and extracellular pH. J. Cell. Physiol. 151, 386–394.

Dimmer, K.-S., Friedrich, B., Lang, F., Deitmer, J.,W., Bröer, S., 2000. The low-affinity monocarboxylate transporter MCT4 ia adapted to the export of lactate in highly glycolytic cells. Biochem. J. 350, 219–227. nuscript in preparation.

Fasano, A., Herrero, M.A., Rocha Rodrigo, M., 2009. Slow and fast invasion waves in a model of acid-mediated tumour growth. Math. Biosci. 220, 45–56.

Folkman, J., Hochberg, M., 1973. Cell-regulation of growth in three dimensions. J. Exp. Med. 138, 745–753.

Freyer, J.P., Sutherland, R.M., 1985. A reduction in the in situ rates of oxygen and glucose consumption of cells in EMT6/Ro spheroids during growth. J. Cell. Physiol. 124, 516–524.

Freyer, J.P., Sutherland, R.M., 1986a. Regulation of growth saturation and development of necrosis in EMT6/Ro multicellular spheroids by the glucose and oxygen supply. Cancer Res. 46, 3504–3512.

Freyer, J.P., Sutherland, R.M., 1986b. Proliferative and clonogenic heterogeneity of cells from EMT6/Ro multicellular spheroids induced by the glucose and oxygen supply. Cancer Res. 46, 3513–3520.

Freyer, J.P., 1988. Role of necrosis in regulating the growth saturation in multicellular spheroids. Cancer Res. 48, 2432–2439

Freyer, J.P., Schor, P.L., Jarret, K.A., Neeman, M., Sillerud, L.O., 1991. Cellular energetics measured by Phosphorous Nuclear Magnetic Resonance spectroscopy are not correlated with chronic nutrient deficiency in multicellular tumor spheroids. Cancer Res. 51, 3831–3837.

Gatenby, R.A., Gawlinski, E.T., 1996. A reaction-diffusion model for cancer invasion. Cancer Res. 56, 5745–5753.

Gerlee, P., Anderson, A.R., 2008. A hybrid cellular automaton model of clonal evolution in cancer: the emergence of the glycolytic phenotype. J. Theor. Biol. 250, 705–722.

Groebe, K., Mueller-Klieser, W., 1991. Distributions of oxygen, nutrient, and metabolic waste concentrations in multicellular spheroids and their dependence on spheroid parameters. Eur. Biophys. J. 19, 169–181.

Guppy, M., Leedman, P., Zu, X.L., Russel, V., 2002. Contribution by different fuels and metabolic pathways to the total ATP turnover of proliferating MCF-7 breast cancer cells. Biochem. J. 364, 309–315.

Hinkle, P.C., Kumar, M.A., Resetar, A., Harris, D.L., 1991. Mechanistic stoichiometry of mitochondrial oxidative phosphorylation. Biochemistry 30, 3576–3582.

Hlatky, L., Sachs, R.K., Alpen, E.L., 1988. Joint oxygen-glucose deprivation as the cause of necrosis in a tumor analog. J. Cell. Physiol. 134, 167–178.

Höchel, M., Vaupel, P., 2001. Tumor hypoxia: definitions and current clinical, biologic, and molecular aspects. J. Nat. Cancer Inst. 93, 266–276.

Jiang, Y., Pjesivac-Grbovic, J., Cantrell, C., Freyer, J.P., 2005. A multiscale model for avascular tumor growth. Biophys. J. 89, 3884–3894.

Li, C.K.N., 1982. The glucose distribution in 9L rat brain multicell tumor spheroids and its effect on cell necrosis. Cancer 50, 2066–2073.

Liuzzi, G., Lucidi, S., Parasiliti, F., Villani, M., 2003. Multi-objective optimization techniques for the design of induction motors. IEEE Trans. Magnetics 39, 1261–1264.

Mueller-Klieser, W., Sutherland, R.M., 1982. Oxygen tensions in multicell spheroids of two cell lines. Br. J. Cancer 45, 256–264.

Mueller-Klieser, W., 1984. Method for the determination of oxygen consumption rates and diffusion coefficients in multicellular spheroids. Biophys. J. 46, 343–348.

Poole, R.C., Halestrap, A.P., 1993. Transport of lactate and other monocarboxylates across mammalian plasma membranes. Am. J. Physiol. 264, C761–C782.

Schaller, G., Meyer-Hermann, M., 2005. Multicellular tumor spheroids in an off-lattice Voronoi/Delaunay cell model. Phis. Rev. E 71, 051 910-051 916.

Schaller, G., Meyer-Hermann, M., 2006. Continuum versus discrete model: a comparison for multicellular tumour spheroids. Phil. Trans. R. Soc. A 364, 1443–1464.

Schroeder, T., Yuan, H., Viglianti, B.L., Peltz C., Asopa, S., Vujaskovic, Z., Dewhirst, M.W., 2005. Spatial heterogeneity and oxygen dependence of glucose consumption in R3230Ac and fibrosarcomas of the Fischer 344 rat. Cancer Res. 65, 5163–5171.

Smallbone, K., Gavaghan, D.J., Gatenby, R.A., Maini, P.K., 2005. The role of acidity in solid tumour growth and invasion. J. Theor. Biol. 235, 476–484.

Smallbone, K., Gatenby, R.A., Gillies, R.J., Maini, P.K., Gavaghan, D.J., 2007. Metabolic changes during carcinogenesis: potential impact on invasiveness. J. Theor. Biol. 244, 703–713.

Spencer, T.L., Lehninger, A.L., 1976. L-lactate transport in Ehrlich ascites-tumour cells. Biochem. J. 154, 405–414.

Stryer, L., 1988 Biochemistry, W.H. Freeman and Company, New York, Chaps. 15–17.

Sutherland, R.M., 1988. Cell and environment interactions in tumor microregions: the multicell spheroid model. Science 240, 177–184.

Swabb, E.A., Wei, J., Gullino, P.M., 1974. Diffusion and convection in normal and neoplastic tissues. Cancer Res. 34, 2814–2822.

Tannock, I.F., 1968. The relation between cell proliferation and the vascular system in a transplanted mouse mammary tumour. Br. J. Cancer 22, 258–273.

Thews, G., Hutten, H., 1983. Biophysics of respiratory gas transport. In: Biophysics (W. Hoppe, H. Lohmann, H. Markl, H. Ziegler, eds.), Springer-Verlag, Berlin, 503–514.

Thomlinson, R.H., Gray, L.H., 1955. The histologic structure of some human lung cancers and the possible implications for radiotherapy. Br. J. Cancer 9, 539–549.

Venkatasubramanian, R., Henson, M.A., Forbes, N.S., 2006. Incorporating energy metabolism into a growth model of multicellular tumor spheroids. J. Theor. Biol. 242, 440–453.

Walenta, S., Dotsch, J., Mueller-Klieser, W., 1990. ATP concentrations in multicellular tumor spheroids assessed by single photon imaging and quantitative bioluminescence. Eur. J. Cell Biol. 52, 389–393.

Walenta, S., Dotsch, J., Mueller-Klieser, W., Kunz-Schughart, L.A., 2000. Metabolic imaging in multicellular spheroids of oncogene-transfected fibroblasts. J. Histochem. Cytochem. 48, 509–522.

Wang, Q., Morris, M.E., 2007. The role of monocarboxylate transporter 2 and 4 in the transport of γ-hydroxybutyric acid in mammalian cells. Drug Metab. Disp. 35, 1393–1399.

Warburg, O., 1956. On the origin of cancer cells. Science 123, 309–314.

Webb, S.D., Sherratt, J.A., Fish, R.G., 1999. Mathematical modelling of tumour acidity: regulation of intracellular pH. J. Theor. Biol. 196, 237–250.

Table 1: Model parameter values

Symbol	Value	Source
F_G	21.5×10^{-17} mol/(cell·s)	assumed
K_G	0.04 mM	(Casciari et al., 1992)
K_O	4.64×10^{-3} mM	(Casciari et al., 1992)
η_1	2.5	(Hinkle et al., 1991)
η_2	1.5	(Hinkle et al., 1991)
D_G	1.05×10^{-6} cm^2/s	(Casciari et al., 1988)
D_L	1.78×10^{-6} cm^2/s	(Casciari et al., 1992)
D_O	1.82×10^{-5} cm^2/s	(Mueller-Klieser, 1984)
D_G^w	9.25×10^{-6} cm^2/s	(Li, 1982)
D_L^w	1.20×10^{-5} cm^2/s	(Swabb et al., 1974)
D_O^w	3.0×10^{-5} cm^2/s	(Thews and Hutten, 1983)
n	2.1×10^8 cells/cm^3	(Freyer and Sutherland, 1986a)
L	80 μm	assumed

Table 2: Parameter estimates and coefficients of variation (CV)

Symbol	Estimate	CV (%)
γ	0.198	—
p_1	18.78×10^{-14} liter/(cell·s)	19.91
f_N	42.82×10^{-17} mol/(cell·s)	0.90

Figure legends

Figure 1. Simplified scheme of glucose metabolism. The inner box represents the mitochondria.

Figure 2. Oxygen consumption rate at $\sigma_L = 1\,\mathrm{mM}$ according to Eq. (10). Parameter values: F_G, K_G and K_O as in Table 1, $p_1 = 10 \cdot 10^{-14}$ liter/(cell·s), $p_2 = 500 \cdot 10^{-17}$ mol/(cell·s), $F_P = 50 \cdot 10^{-17}$ mol/(cell·s).

Figure 3. Maximal value of the oxygen consumption rate as a function of σ_G and σ_L. Parameter values as in Fig. 2.

Figure 4. Lactate consumption/production rate as a function of oxygen concentration for three values of lactate concentration. Left panel, $\sigma_G = 0$; right panel, $\sigma_G = 5\,\mu\mathrm{M}$. Other parameters as in Fig. 2.

Figure 5. Fraction of ATP production (computed with $\sigma_G = 5\,\mu\mathrm{M}$, $\sigma_O = 0.28\,\mu\mathrm{M}$ and $\sigma_L = 1\,\mu\mathrm{M}$) due to the glycolytic step as a function of F_P for three values of p_2. Other parameters as in Fig. 2.

Figure 6. Optimal prediction of the radius of the necrotic core as a function of the spheroid radius, together with the experimental measurements reported in Freyer and Sutherland, 1986 (courtesy of Dr. J.P. Freyer). Left panel, oxygen concentration in medium 0.07 mM; right panel, oxygen concentration in medium 0.28 mM. Glucose concentrations are reported in the inset. The estimated values of the parameters p_1, γ and f_N are given in Table 2, other parameters reported in Table 1.

Figure 7. Predicted profiles of glucose, lactate and oxygen concentrations and of ATP production rate as a function of the radial distance in a spheroid of radius $R = 400\,\mu\mathrm{m}$ cultured with 5.5 mM glucose and 0.28 mM oxygen. The concentrations in the unstirred layer ($L = 80\,\mu\mathrm{m}$) are shown. The necrotic radius is $\rho_N = 209.38\,\mu\mathrm{m}$. The values of p_1, γ and f_N are given in Table 2, other parameters reported in Table 1.

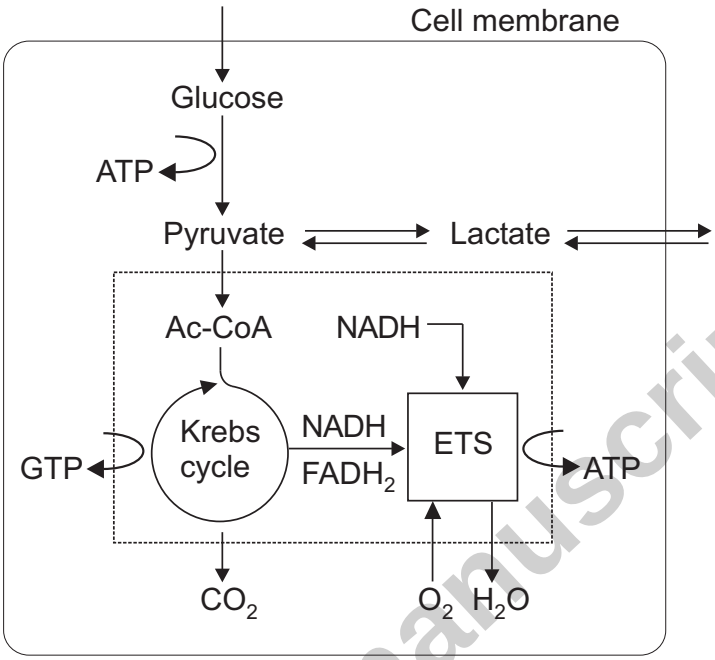

Figure 1:

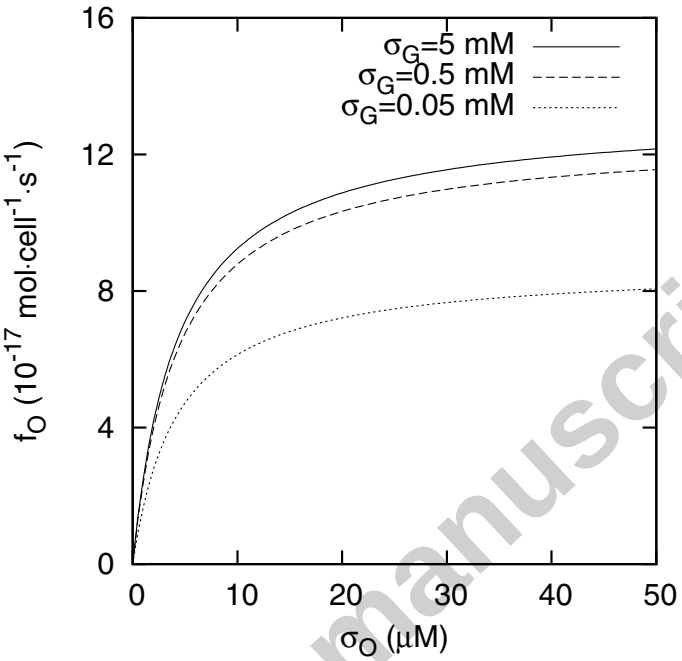

Figure 2:

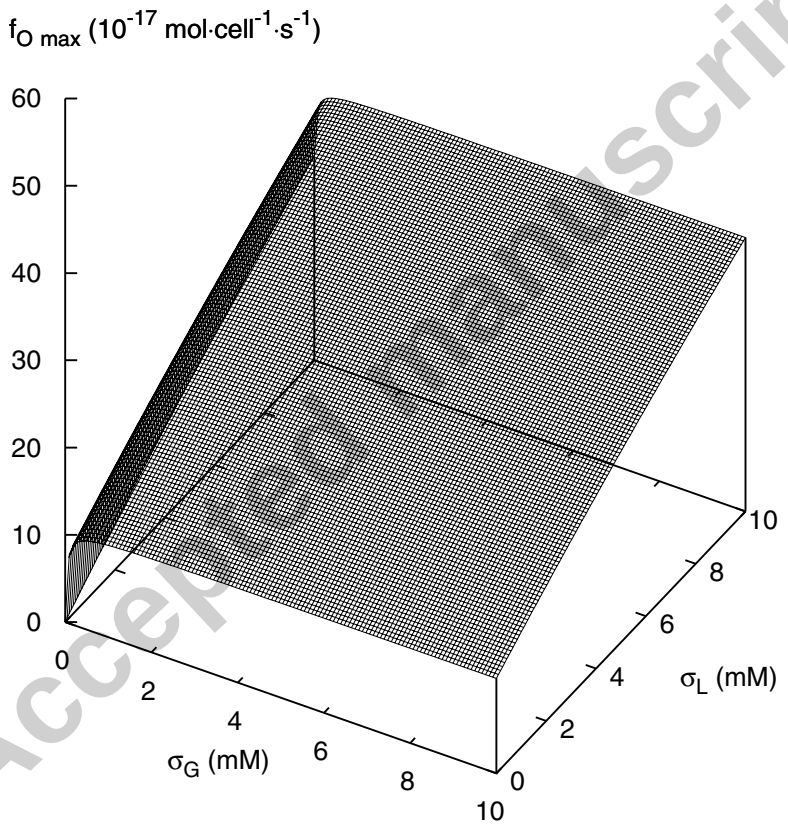

Figure 3:

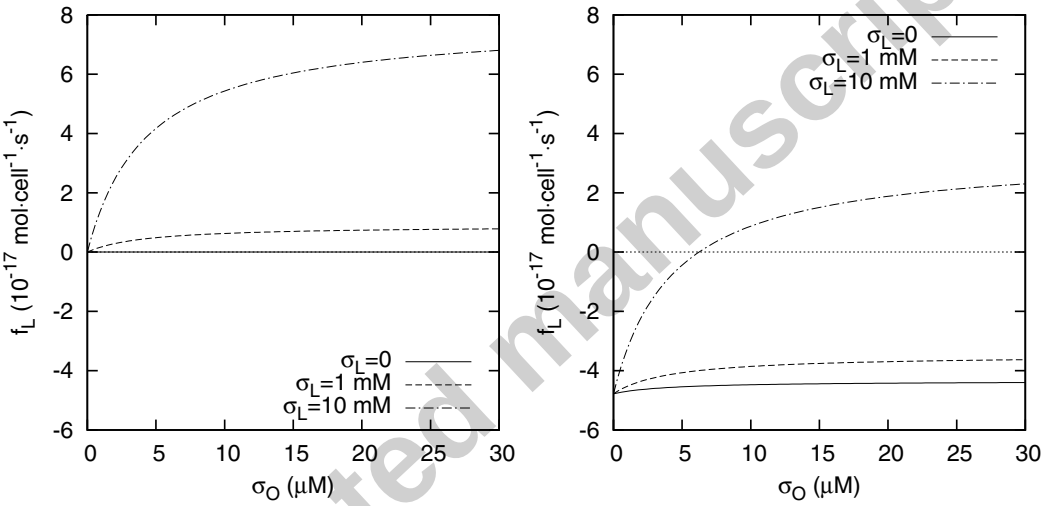

Figure 4:

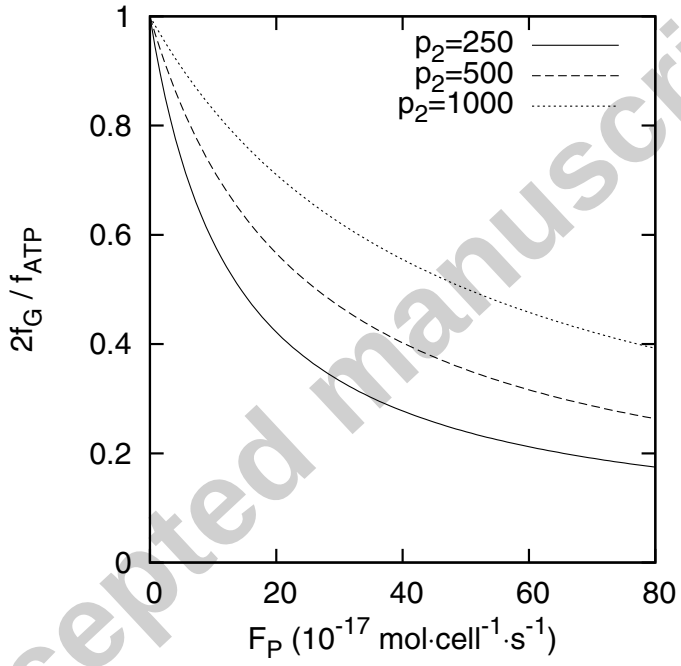

Figure 5:

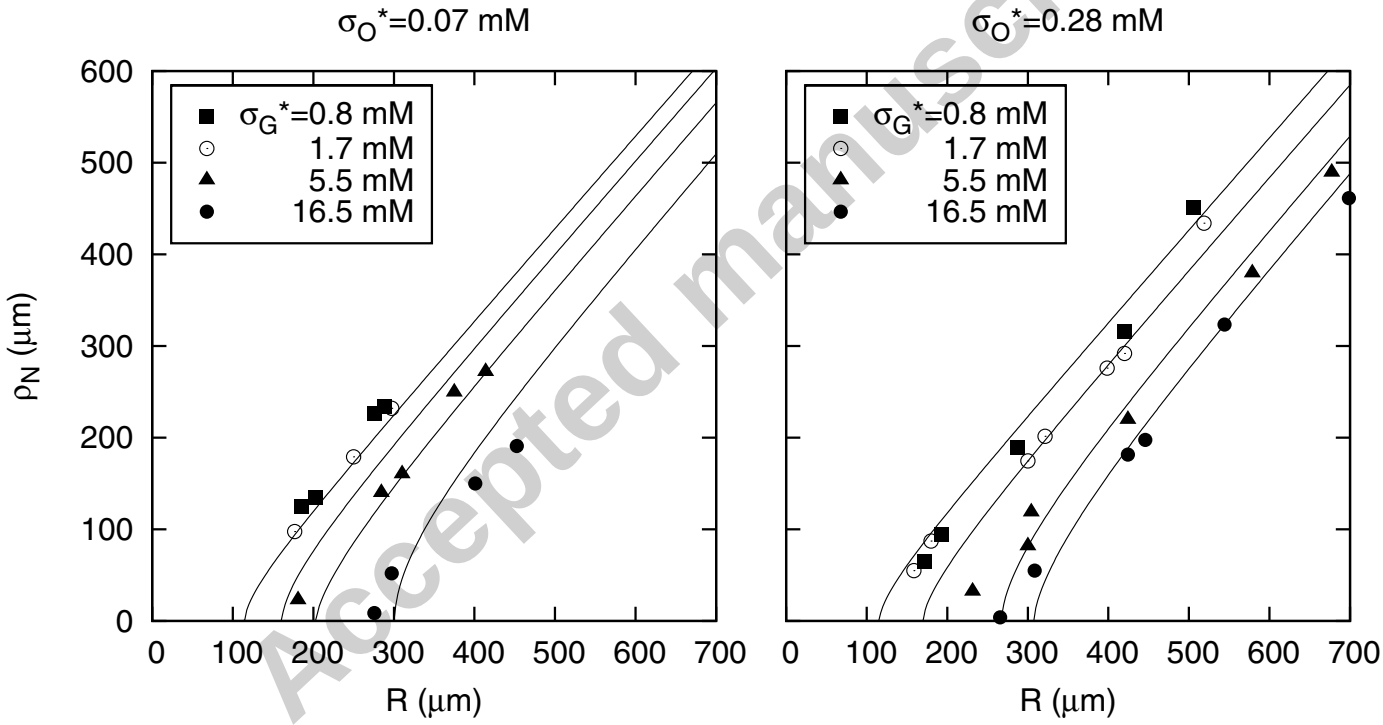

Figure 6:

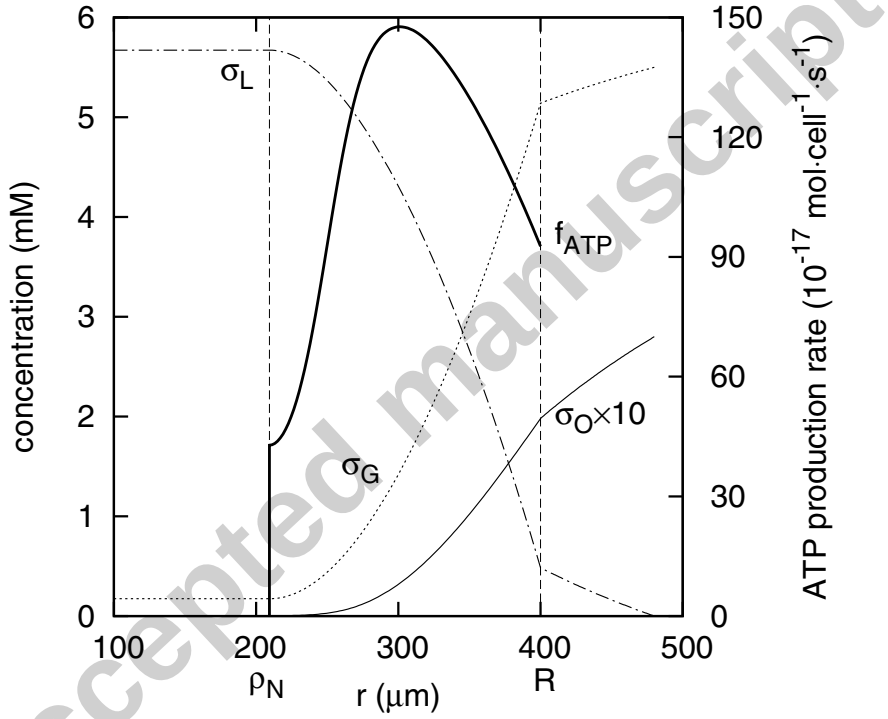

Figure 7: